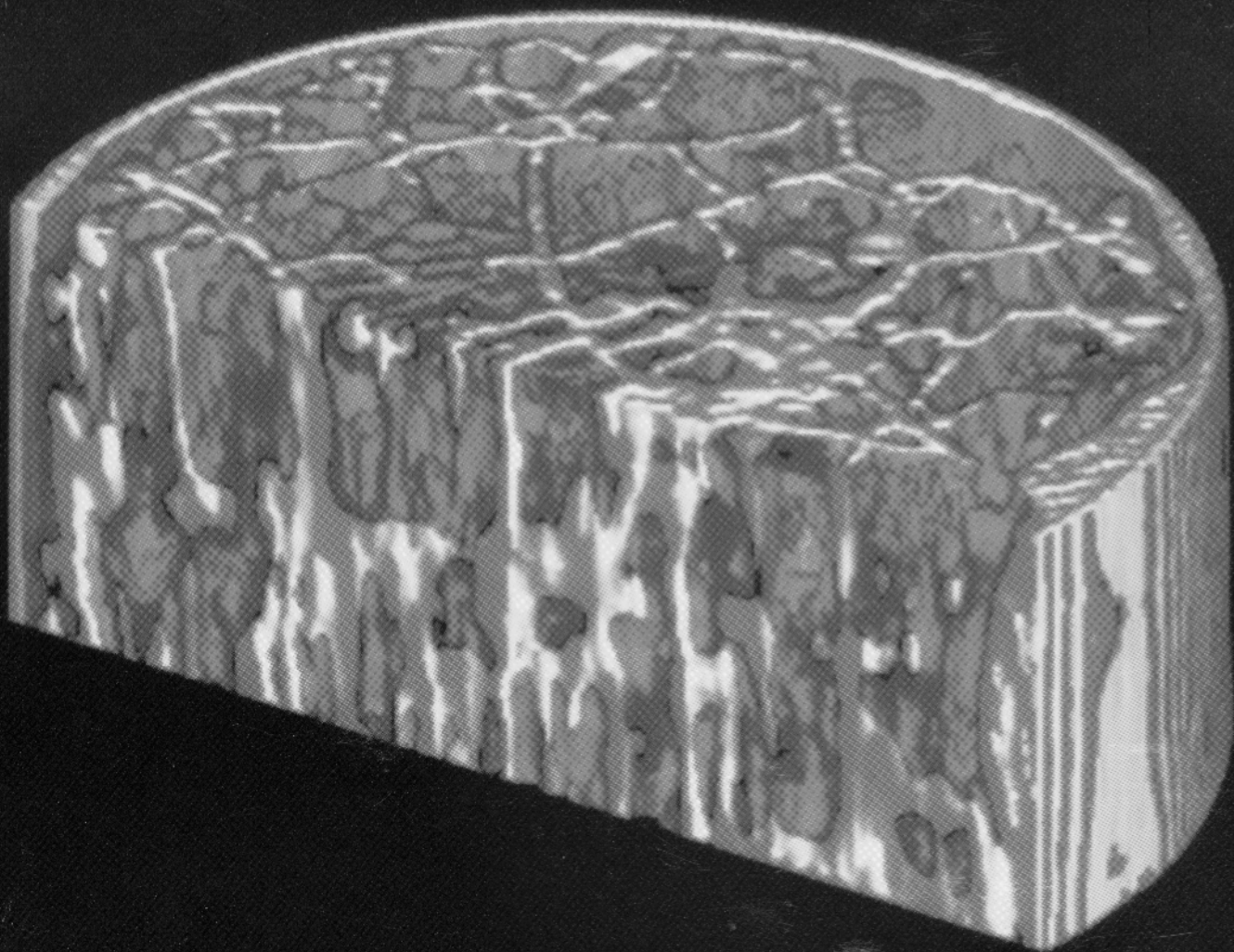


Geophysical  
Research  
Letters



JUNE 1, 1995

Volume 22 Number 11

AMERICAN GEOPHYSICAL UNION

## Porosity of natural fracture networks

Carlo D. Montemagno

Argonne National Laboratory, Argonne, Illinois

Laura J. Pyrak-Nolte

Department of Civil Engineering and Geological Sciences, University of Notre Dame, Notre Dame, Indiana

**Abstract.** Volumetric imaging is used to determine the three-dimensional topology of natural fracture networks in coal subjected to reservoir conditions. Computerized X-ray tomographic data and bulk porosity measurements are combined with image processing techniques to quantify the porosity distribution of three-dimensional fracture networks in two coal cores. Under in-situ conditions, the porosity of the fracture networks in the cores is less than one-tenth of a percent. In addition, the porosity varies by  $\pm 10\%$  over depth intervals of approximately 16 mm.

### Introduction

The transport of fluids through a fractured rock mass is intimately related to the geometry of the fracture network. Numerical models for simulating fluid flow through a fracture network in three dimensions require data on the geometry of the network, such as spatial correlations, interconnectivity, fracture aperture, fracture length and orientation (Long et al., 1985 & 1991). While the flow models are sophisticated, direct data on the three-dimensional topology of fracture networks have been lacking. Typically, the geometry of real fracture networks are only measurable as two-dimensional planes or cross-sections, such as in rock outcrops, tunnel or excavation walls, or as thin sections after destruction of a rock sample. The difficulty in characterizing natural fracture networks in rock arises because three-dimensional networks are imbedded in a rock matrix that is opaque to almost all probes. Advanced seismic techniques are currently being studied as a means of remote non-destructive detection of fractures (Pyrak-Nolte, 1990; Nihei et al, 1994). However, significantly more theoretical and technological development is needed to reconstruct the complex three-dimensional network geometry of natural fracture systems using seismic analysis.

An integrated fracture measurement and analysis system has been developed to examine the relationship between fracture network geometry and the physical properties of the medium. In this paper, we use X-ray computerized tomography (CT) analysis and three-dimensional image analysis to investigate the three-dimensional geometry of fracture networks in coal, and measure the variation in porosity of the connected fracture network as a function of distance along the core axis.

Copyright 1995 by the American Geophysical Union.

Paper number 95GL01098  
0094-8534/95/95GL-01098\$03.00

### Experimental Technique

Two coal cores were used in this investigation. Coal cores AA and BB were drilled from blocks of coal from Seam #1 in the Sundance Pit at the La Plata coal mine, San Juan County, New Mexico (Pyrak-Nolte et al., 1993). Core AA was drilled perpendicular to the bedding planes while Core BB was drilled parallel to the bedding planes and to the prominent fracture orientation.

The bulk porosity of the fracture network was measured using two techniques: a helium-water drive method, and a metal injection method. In the helium-water drive, the coal core is saturated with brine that is subsequently displaced with humidified helium. The volumes of helium and brine produced are recorded and used to establish the porosity of the sample (Gash, 1991; Gash et al., 1992). A Wood's metal injection method was used to capture the geometry of natural fracture networks under in-situ reservoir conditions. The high surface tension of Wood's metal (Table 1) enables the size of fracture aperture accessed to be controlled by the injection pressures, and ensures that the injected metal conforms to the geometry of the void space. In addition, the Wood's metal in the fractures provides a large density contrast between the rock matrix and the metal-filled fractures. X-ray computerized tomography (CT) utilizes the density difference between the coal matrix and the Wood's-metal filled fractures to image the three-dimensional geometry of the fracture networks.

To inject a coal sample with Wood's metal (Pyrak-Nolte, 1991), the sample is placed in a hydrostatic pressure vessel and subjected to the desired stress. The sample is heated to 95 °C while a nitrogen back pressure is maintained. The nitrogen back pressure reduces the potential for oxidation of the coal and provides a constant pressure front for the invading metal. The confining pressure and nitrogen pressure used for each core are given in Table 2. When the sample has reached the desired temperature, metal is injected into the sample. After injection, the sample is allowed to cool causing the metal to solidify and form a metal cast of the fracture network. Gravimetric measurements are used to determine the metal-filled void volume and to calculate effective network porosity. Computerized x-ray tomography (CT) of the metal-filled coal specimens provides information on the geometry of the network such as number of fractures and fracture orientation. For coal cores AA and BB, 42 and 92 CT slices were taken respectively. The CT slices represent sections 1.05 mm and 1.217 mm in thickness for cores AA and BB, respectively.

### Results from Wood's Metal Method

Table 2 contains the results of the Wood's metal injection experiments. The volume of metal injected divided by the bulk

Table 1. Properties of Wood's Metal (Cerrosafe®)

Components:	
Bismuth	42.5 %
Lead	37.7 %
Tin	11.3 %
Cadmium	8.5 %
Melting Temperature Range (°C)	70 °C - 88 °C
Surface Tension (dynes/cm)	485 ± 17
Density (gram/cm <sup>3</sup> )	9.8
Contact Angle on Coal	130° + 21°
Young's Modulus (GPa)	9.7

volume of the sample gives the porosity of the fracture network. The porosity of the fracture network determined from the Wood's metal method is less than the porosity determined from the helium-water drive (Table 3). Because of the high surface tension of Woods metal, the size of the pores accessed is limited to pores larger in size than the pores accessed by helium. For Core AA and Core BB, the Wood's metal method yields the porosity of the fracture network for apertures greater than 2 microns. However, both techniques yield a fracture network porosity on the order of one-tenth of a percent.

### Image Analysis

In addition to the data from the Wood's metal method and the helium-water drive, the x-ray computerized tomographic images yield information on the geometry of the fracture network. To study the variation of porosity with depth, image processing was performed to determine the aperture size of the fractures in the network. Because the x-ray sources of CT

Table 2. Data from Wood's Metal Injection Experiments on Coal Samples AA and BB from Seam #1 in the Sundance Pit at the La Plata Coal Mine, San Juan County, New Mexico

Sample Number	AA	BB
Orientation of Drill Core	Perpendicular to Bedding Planes	Parallel to Face Cleat & Bedding Planes
Sample Dimensions:		
Diameter (cm)	8.89	8.89
Length (cm)	4.41	11.2
Bulk Volume (cm <sup>3</sup> )	274	694
Confining Pressure at Solidification (MPa)	4.89	5.54
Nitrogen Pressure at Solidification (MPa)	0.49	0.44
Weight of Injected Wood's Metal (grams)	2.14	6.19
Radius of the Minimum Aperture Filled with Wood's Metal <sup>1</sup> (μm)	1.22 ± 0.59	1.37 ± 0.65
Volume of Connected Voids with Aperture ≥ Minimum Aperture Accessed <sup>2</sup> (cm <sup>3</sup> )	0.22 ± 0.005	0.65 ± 0.013
Effective Fracture Porosity <sup>2</sup> (%)	0.082 ± 0.002	0.094 ± 0.002

<sup>1</sup>Error from deviations in surface tension and contact angle of Wood's metal <sup>2</sup>Error from deviations in the density of Wood's metal

Table 3. Comparison of porosity (%) measurements using different methods

Measurement Method	AA	BB
Unsteady-State	0.22	0.11
Gravimetric	0.082	0.094

scanners typically do not produce a monochromatic beam of photons, selective attenuation of photons of different energies results in the generation of beam hardening artifacts (Kak & Slaney, 1988) that are clearly evident in the reconstructed two-dimensional images (Figure 1). These artifacts are most pronounced in regions with a highest density gradient, such as the interface between the Wood's metal-filled fracture and the coal matrix. In these experiments, beam hardening reduced the achievable resolution of the two-dimensional CT scans from 0.3 mm to greater than 1 mm.

Visual examination of a Wood's metal-filled coal core established that the fracture aperture is typically less than 0.1 mm, much less than the optimal 0.3 m resolution of the CT scanner. Because each fracture aperture is less than the resolution of the CT images, a 0.3 mm by 0.3 mm pixel can only establish whether or not a fracture intersects the pixel. The geometry of a fracture aperture cannot be directly resolved. However, because the fracture apertures were smaller than the dimensions of one pixel, the imaged fractures were reduced using an erosion and dilation morphological procedure (Jain, 1989) to a width of 1 pixel within each two-dimensional scan and the position of each fracture was established to an accuracy of 0.3 mm (Figure 2).

To determine the porosity of each CT slice, the aperture of the fractures were determined using the density and spatial location information from the CT data. The natural log of the magnitude of absorption (or CT number, CT<sub>#</sub>) of an x-ray beam is linearly proportional to the thickness of the absorbing material. Using this relation, a constant of proportionality, F, was calculated to relate the CT<sub>#</sub> to the volume density of metal within a voxel using equation 1.

$$\sum_N \text{Voxel Volume} * CT_N * F = (\text{Reconstructed Volume/Bulk Volume}) * \text{Volume of Metal Injected} \quad \text{eq}(1).$$

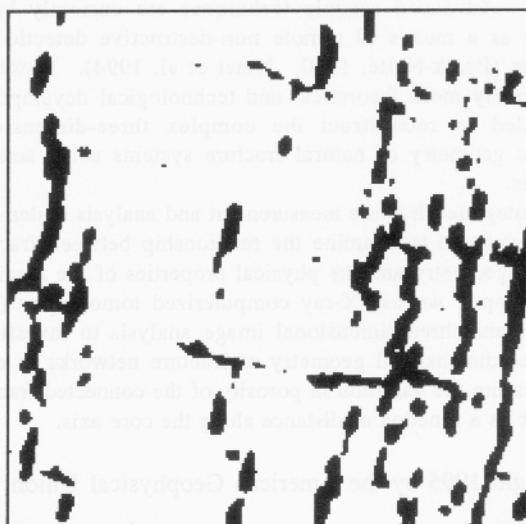
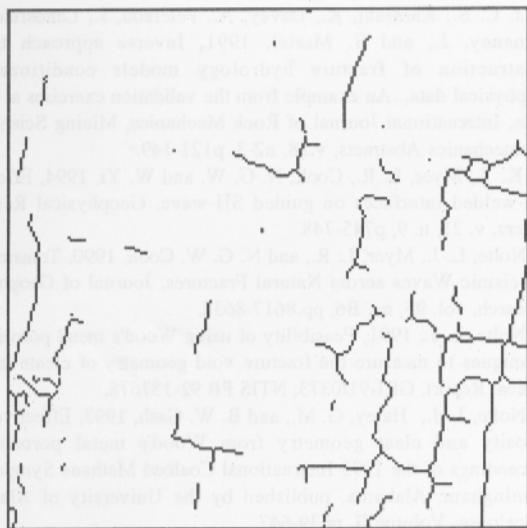


Figure 1. Preprocessed CT image of a two-dimensional fracture network



**Figure 2.** Two-dimensional CT image of a fracture network processed to remove beam hardening artifacts.

For cores AA and BB, the coefficient  $F$  had values of  $1.45 \times 10^{-5}$  and  $1.92 \times 10^{-5}$ , respectively. The measured volume of the fracture network from the Wood's metal experiments constrains the porosity of the CT images, i.e. it limits the size of the apertures of the fractures. The calculated volume densities were remapped to the appropriate locations within the fracture network to provide an average fracture aperture for each pixel in the CT images that contained a fracture. The sum of the metal volume densities is equivalent to the effective fracture network porosity.

Figure 3 shows the histogram per slice of porosity for Core AA and Core BB determined from the CT images of the fracture

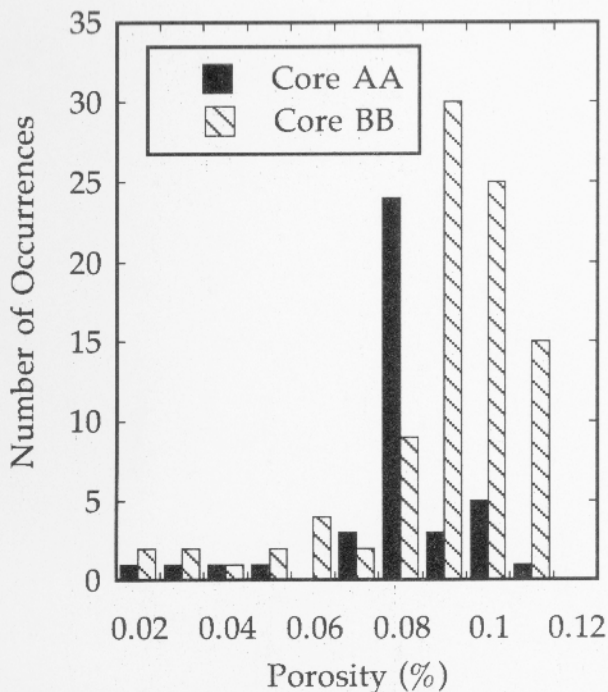


**Figure 3.** Histogram illustrating the distribution of porosity for coal cores AA and BB.

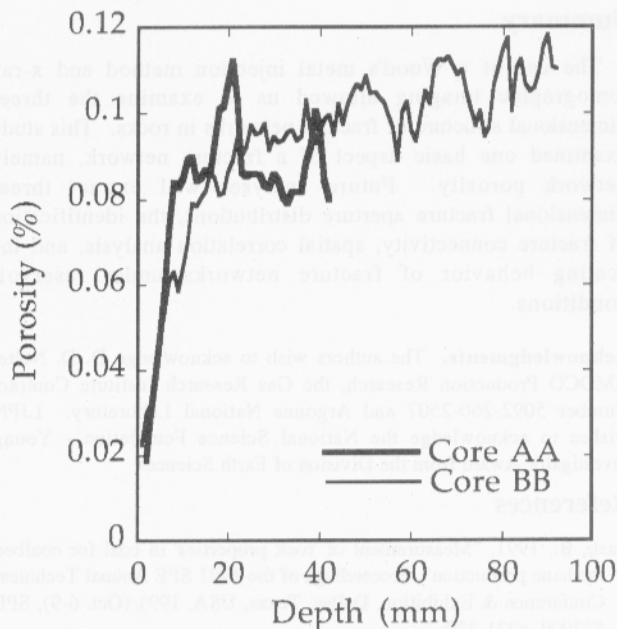


**Figure 4.** Plot of the variation of porosity as a function of depth in coal cores AA and BB.

network. For both cores, the porosity per slice ranged from 0.02% to 0.11%. Core AA has a mean porosity of  $0.080\% \pm 0.022\%$ . For Core BB, the mean porosity is  $0.094\% \pm 0.0195\%$ . The distribution of porosity is strongly peaked around the average value, but has a broad low tail from low porosity. This indicates that some slices had anomalously low porosities. To obtain a better understanding of the range of porosities slice to slice and the variability for two adjacent slices, it is necessary to track the porosity as a function of position along the length of the core.

Figure 4 shows the variation of porosity with depth for both samples. The very low porosities at shallow depths (0 - 8 mm for Core AA, and 0-12 mm for Core BB) correspond to the outlet side of the sample during injection and indicate that these portions of the samples were not fully injected. For positions in the cores away from these shallow depths, the porosity maintains an average value with fluctuations that vary over several millimeters. Within this relatively constant range, when the rapid drop-off at the exit is excluded from the data set, the porosities of Core AA and Core BB are  $0.0886\% \pm 0.00823\%$  and  $0.0997\% \pm 0.00941\%$ , respectively. The porosity fluctuation is approximately  $\pm 10\%$  of the average value. The fluctuations reflect changes in the geometry of the fracture network, specifically aperture and interconnectivity. The one dimensional correlation length was used to examine the spatial persistence of the porosity fluctuations. Core AA is uncorrelated along the length of the core which indicates that either the fracture network is not correlated in this direction or that the sample is smaller than the correlation length. Analysis of other coal cores from the same basin for the same orientation of perpendicular to bedding planes (Pyrak-Nolte et al., 1995) exhibited correlation lengths on the order of 4 mm to 5 mm. Core BB had a correlation length of 16 mm along the axis of the core recognizing that core BB was oriented parallel to the bedding planes. This illustrates the structural heterogeneity of the fracture network and presents a qualitative indication of the length scale over which interconnectivity is maintained.

Summary

The use of a Wood's metal injection method and x-ray tomographic imaging allowed us to examine the three-dimensional structure of fracture networks in rocks. This study examined one basic aspect of a fracture network, namely network porosity. Future analyses will extract three-dimensional fracture aperture distributions, the identification of fracture connectivity, spatial correlation analysis, and the scaling behavior of fracture networks under reservoir conditions.

**Acknowledgments.** The authors wish to acknowledge D. D. Nolte, AMOCO Production Research, the Gas Research Institute Contract Number 5092-260-2507 and Argonne National Laboratory. LJPN wishes to acknowledge the National Science Foundation - Young Investigator Award from the Division of Earth Sciences.

References

Gash, B., 1991, "Measurement of 'rock properties' in coal for coalbed methane production", Proceedings of the 1991 SPE Annual Technical Conference & Exhibition, Dallas, Texas, USA, 1991 (Oct. 6-9), SPE #22909, p221-230.

Gash, B., Volz, R.F., Gary, P., and J. M. Corgan, 1992, The effect of cleat orientation and confining pressure on cleat porosity, permeability and relative permeability in coal, 1992 SCCA Conference paper no. 9224, June, 1992, Tulsa, Oklahoma.

Jain, A. K., 1989, Fundamentals of Digital Image Processing, Prentice Hall, New Jersey.

Kak, A. C. and M. Slaney, 1988, Principles of Computerized Tomographic Imaging, IEEE Press, New York.

Long, J. C. S. and Witherspoon, P. A., 1985, The Relationship of the Degree of Interconnection to Permeability in Fracture Networks, JGR, Vol. 90, pp. 3087-3098.

Long, J. C. S., Karasaki, K., Davey, A., Peterson, J., Landsfeld, M., Kemeny, J., and S. Martel, 1991, Inverse approach to the construction of fracture hydrology models conditioned on geophysical data. An example from the validation exercises at Stripa mine, International Journal of Rock Mechanics, Mining Sciences & Geomechanics Abstracts, v.28, n2-3, p121-149.

Nihei, K. T., Myer, L. R., Cook, N. G. W. and W. Yi, 1994, Effects of non-welded interfaces on guided SH-wave, Geophysical Research Letters, v. 21, n. 9, p745-748.

Pyrak-Nolte, L. J., Myer, L. R., and N. G. W. Cook, 1990, Transmission of Seismic Waves across Natural Fractures, Journal of Geophysical Research, vol. 95, no. B6, pp.8617-8638.

Pyrak-Nolte, L. J., 1991, Feasibility of using Wood's metal porosimetry techniques to measure the fracture void geometry of cleats in coal, Topical Report, GRI-91/0373; NTIS PB 92-137678.

Pyrak-Nolte, L. J., Haley, G. M., and B. W. Gash, 1993, Effective cleat porosity and cleat geometry from Wood's metal porosimetry, Proceedings of the 1993 International Coalbed Methane Symposium, Birmingham, Alabama, published by the University of Alabama, Tuscaloosa, Volume II, p639-647.

Pyrak-Nolte, L. J., G. Yang, C. Montemagno, L. Myer, and N. G. W. Cook, 1995, Three-dimensional tomographic visualization of natural fractures and graph theory analysis of the transport properties, Proceedings of the 8th International Congress of Rock Mechanics, A. A. Balkema, Rotterdam.

Prof. Laura J. Pyrak-Nolte, Department of Civil Engineering and Geological Sciences, University of Notre Dame, Notre Dame, Indiana 46556-0767 (e-mail: pyrak-nolte@nd.edu)

Dr. Carlo D. Montemagno, Argonne National Laboratory, Argonne, Illinois 60439 (e-mail: cmontema@hawk.ce.nd.edu)

(Received January 11, 1995; accepted February 22, 1995)



REGULAR SECTION

- Cenozoic plate driving forces** (Paper 95GL01325) 1317  
*C. Lithgow-Bertelloni and Mark A. Richards*
- Aftershock distribution of the October 4, 1994 Mw8.3 Kurile Islands earthquake determined by a local seismic network in Hokkaido, Japan** (Paper 95GL01316) 1321  
*K. Katsumata, M. Ichiyanagi, M. Miwa, M. Kasahara, and H. Miyamachi*
- Observation of pressure change associated with hydrothermal upwelling at a seamount in the south Mariana Trough using an ocean bottom seismometer** (Paper 95GL01314) 1325  
*Toshinori Sato, Junzo Kasahara, and Kantaro Fujioka*
- Wavelet analysis of velocity dispersion of elastic interface waves propagating along a fracture** (Paper 95GL01323) 1329  
*Laura J. Pyrak-Nolte and David D. Nolte*
- Tree-ring evidence of the widespread effects of explosive volcanic eruptions** (Paper 94GL03113) 1333  
*P. D. Jones, K. R. Briffa, and F. H. Schweingruber*
- Superparamagnetism and reduction diagenesis in pelagic sediments: Enhancement or depletion?** (Paper 95GL00888) 1337  
*John A. Tarduno*
- Magnetic stratigraphy of Chinese loess as a record of natural fires** (Paper 95GL01324) 1341  
*Günther Kletetschka and Subir K. Banerjee*
- Recent variations in mean temperature and the diurnal temperature range in the Antarctic** (Paper 95GL01198) 1345  
*P. D. Jones*
- Observations of ultraviolet light reflection and transmission by first-year sea ice** (Paper 95GL01062) 1349  
*Donald K. Perovich*
- Assessment of the SAGE sampling strategy in the derivation of tropospheric water vapor distribution in a general circulation model** (Paper 95GL01336) 1353  
*M. H. Zhang*
- Visible contrail formation from fuels with different sulfur contents** (Paper 95GL01312) 1357  
*R. Busen and U. Schumann*
- A spectroradiometer for the measurement of direct and scattered solar irradiance from on-board the NASA ER-2 high-altitude research aircraft** (Paper 95GL01391) 1361  
*C. T. McElroy*
- A comparison of J-values from the composition and photodissociative flux measurement with model calculations** (Paper 95GL01392) 1365  
*C. T. McElroy, C. Midwinter, D. V. Barton, and R. B. Hall*
- Observed stratospheric profiles and stratospheric lifetimes of HCFC-141b and HCFC-142b** (Paper 95GL01313) 1369  
*J. M. Lee, W. T. Sturges, S. A. Penkett, D. E. Oram, U. Schmidt, A. Engel, and R. Bauer*
- Detection of HBr and upper limit for HOBr: Bromine partitioning in the stratosphere** (Paper 95GL01349) 1373  
*D. G. Johnson, W. A. Traub, K. V. Chance, and K. W. Jucks*

(continued on inside back cover)

---

**Cover.** A three-dimensional rendering of the unprocessed x-ray tomographic scans from a coal core with metal-filled fractures. The blue regions represent the coal matrix and the yellow regions represent the fracture positions (see paper by Montemagno and Pyrak-Nolte [this issue]).

---